Original Article

Microvascular fragment spheroids: Three-dimensional vascularization units for tissue engineering and regeneration

Journal of Tissue Engineering
Volume 12: 1–13

DOI: 10.1177/20417314211035593
journals.sagepub.com/home/tej
SAGE

Lisa Nalbach[1]*, Danièle Müller[1]*, Selina Wrublewsky[1], Wolfgang Metzger[2], Michael D Menger[1], Matthias W Laschke[1] and Emmanuel Ampofo[1]

Abstract

Adipose tissue-derived microvascular fragments (MVF) serve as vascularization units in tissue engineering and regenerative medicine. Because a three-dimensional cellular arrangement has been shown to improve cell function, we herein generated for the first time MVF spheroids to investigate whether this further increases their vascularization potential. These spheroids exhibited a morphology, size, and viability comparable to that of previously introduced stromal vascular fraction (SVF) spheroids. However, MVF spheroids contained a significantly higher number of CD31-positive endothelial cells and α-smooth muscle actin (SMA)-positive perivascular cells, resulting in an enhanced angiogenic sprouting activity. Accordingly, they also exhibited an improved in vivo vascularization and engraftment after transplantation into mouse dorsal skinfold chambers. These findings indicate that MVF spheroids are superior to SVF spheroids and, thus, may be highly suitable to improve the vascularization of tissue defects and implanted tissue constructs.

Keywords

Microvascular fragments, stromal vascular fraction, spheroid, vascularization, angiogenesis, tissue engineering

Received: 4 February 2021; accepted: 12 July 2021

Introduction

In the last decades, several strategies to promote tissue vascularization have been established including conditioned media,[1] microspherical scaffolds,[2] and spheroids.[3] The latter are multi-cellular aggregates with dense cell-cell contacts, which are widely used in cancer research and drug screening, because they mimic the three-dimensional environment of natural tissues.[4] In addition, they have been proposed as vascularization units in angiogenesis research and regenerative medicine.[5] For this purpose, Alajati et al.[6] generated monoculture spheroids consisting of human umbilical vein endothelial cells (HUVEC), which were embedded in a Matrigel-fibrin matrix, to support tissue repair processes. However, the paracrine microenvironment provided by the communication of endothelial cells with other vascular-supporting cell types is of major importance for the formation of a stable, functional microvasculature. Taking this into account, more recent experimental approaches focused on the generation of spheroids consisting of endothelial cells in combination with mesenchymal stem cells,[7] induced pluripotent stem cells (iPSC)[8] or pericytes.[9]

Endothelial cells and pericytes bear the major disadvantage that they cannot be harvested in large quantities under

[1]Institute for Clinical & Experimental Surgery, Saarland University, Homburg, Germany
[2]Department of Trauma, Hand and Reconstructive Surgery, Saarland University, Homburg, Germany

*These authors contributed equally to this work.

Corresponding author:
Emmanuel Ampofo, Institute for Clinical & Experimental Surgery, Saarland University, Kirrberger Straße 100, Homburg/Saar 66421, Germany.
Email: emmanuel.ampofo@uks.eu

Table 1. Antibodies utilized for immunohistochemistry and flow cytometry.

Target	Number	Dilution	Company
Antibodies			
CD31	DIA310	1:200	Dianova (Hamburg, Germany)
Ki67	12202	1:100	Cell Signaling (Danvers, USA)
casp-3	9661	1:200	Cell Signaling (Danvers, USA)
α-SMA	1A4	1:200	Sigma-Aldrich (Taufkirchen, Germany)
MPO	ab9535	1:200	Abcam (Cambridge, UK)
CD117	550741	1:50	BD (Heidelberg, Germany)
CD73	567471	1:50	BD (Heidelberg, Germany)
CD29	562801	1:50	BD (Heidelberg, Germany)
Anti-mouse IgG (H + L)-Cy3		1:1000	Jackson Immuno Research Labs (West Grove, USA)
Anti-rabbit IgG (H + L)-Cy3		1:1000	Jackson Immuno Research Labs (West Grove, USA)
Anti-rat IgG (H + L)-Cy3)		1:1000	Jackson Immuno Research Labs (West Grove, USA)

clinical conditions.[10] To overcome this problem, spheroids may be generated by the fusion of the stromal vascular fraction (SVF). The SVF is a suspension of single endothelial cells, pericytes, macrophages, stromal, and progenitor cells, which can be isolated from patients by enzymatic digestion of adipose tissue.[11] Several studies already reported that SVF supports tissue revascularization along with the secretion of the angiogenic factors including vascular endothelial growth factor (VEGF) and hepatic growth factor (HGF).[12–14] Recently, Muller et al.[15] showed that SVF spheroids exhibit a high angiogenic potential and promote the formation of new blood vessels after in vivo transplantation.

In contrast to the long digestion (~60 min) of adipose tissue for the isolation of the SVF, a markedly shorter digestion (~10 min) yields microvascular fragment (MVF) isolates representing a randomized mixture of non-digested functional arterioles, capillaries, and venules as well as single cells.[16–18] Of interest, MVF have a higher angiogenic potential when compared SVF, because they rapidly reassemble into new microvascular networks and develop interconnections with the host microvasculature after transplantation into tissue defects.[19,20] However, whether MVF are also capable of forming functional spheroids and whether these spheroids are superior to SVF spheroids has not been investigated so far.

Based on these findings, we generated in the present study for the first time MVF spheroids by means of the liquid overlay technique and compared their vascularization potential with that of SVF spheroids, which served as controls. For this purpose, we analyzed the morphology, viability, cellular composition, and angiogenic activity of both spheroid types in vitro. Moreover, we transplanted MVF and SVF spheroids onto the striated muscle tissue within mouse dorsal skinfold chambers to study their vascularization using intravital fluorescence microscopy.

Materials and methods

Reagents

Agarose was purchased from Promega (Dübendorf, Switzerland) and Accutase® from BioLegend (Koblenz, Germany). Trypsin and collagenase NB4G were purchased from SERVA Elektrophoresis GmbH (Heidelberg, Germany). Dulbecco's Modified Eagle's Medium (DMEM) was purchased from PAN Biotech (Aidenbach, Germany). Fluorescein isothiocyanate (FITC)-labeled dextran 150,000, Hoechst 33342, Oil Red O and penicillin were purchased from Sigma-Aldrich (Taufkirchen, Germany). HepatoQuick® was purchased from Roche (Basel, Switzerland). Ketamine (Ursotamin®) was purchased from Serumwerke Bernburg (Bernburg, Germany). Streptavidin-POD was purchased from New England Biolabs (Ipswich, USA) and xylazine (Rompun®) was purchased from Bayer (Leverkusen, Germany). Mayer's hemalum was purchased from Merck (Darmstadt, Germany).

Antibodies

Antibodies used in this study are listed in Table 1.

Animals

Male C57BL/6N mice (Institute for Clinical & Experimental Surgery, Saarland University, Homburg, Germany) in the age of 7–12 months and a body weight of 30–35 g served as donors for the isolation of MVF and the SVF. Dorsal skinfold chambers were implanted in C57BL/6N mice with an age of 3–4 months and a body weight of 24–27 g. Animals were kept on a standard 12/12 h day/night cycle. Water and standard pellet chow (Altromin, Lage, Germany) were provided ad libitum.

All experiments were performed according to the German legislation on protection of animals and the National Institutes of Health (NIH) Guide for the Care and Use of Laboratory Animals (Institute of Laboratory Animal Resources, National Research Council, Washington DC, USA). The experiments were approved by the local governmental animal protection committee (permission number: 18/2017).

Isolation of MVF and SVF single cells

The isolation of MVF was performed as previously described in detail.[16] Briefly, 15 donor mice were anesthetized by an intraperitoneal injection of ketamine (75 mg/kg body weight; Ursotamin®) and xylazine (25 mg/kg body weight; Rompun®). The epididymal fat pads (~0.85 mg per mouse) were harvested, washed, and mechanically dissected before the tissue was enzymatically digested by collagenase NB4G (0.5 U/mL) for 10 min (Figure 1(a)). Subsequently, the MVF isolate consisting of ~55,000 MVF and ~825,000 single cells per mL adipose tissue was washed and kept in DMEM supplemented with 10% (v/v) fetal bovine serum (FBS), 100 U/mL penicillin and 0.1 mg/mL streptomycin at 37°C and 5% CO_2 for the generation of MVF spheroids.

For the isolation of SVF single cells from 15 donor mice, MVF isolates were generated as described above. To completely disperse the MVF into single cells, they were enzymatically digested in a second step by 4% trypsin (0.5 U/mL) for additional 10 min. Finally, the cell suspension was filtered through a 20 µm mesh to remove remaining undigested tissue fragments before the single cells were washed and kept in DMEM supplemented with 10% (v/v) FBS, 100 U/mL penicillin and 0.1 mg/mL streptomycin at 37°C and 5% CO_2 for the generation of SVF spheroids.

Generation of spheroids

MVF and SVF spheroids were generated by means of the liquid overlay technique in a 96-well plate covered with 1% agarose.[21] The wells were equilibrated with culture medium for 1 h at 37°C prior cell seeding. Subsequently, ~1000 MVF (each consisting of ~15 cells) and ~15,000 single cells were seeded per well and cultivated for 5 days to allow the formation of one spheroid at 37°C under a humidified 95% to 5% (v/v) mixture of air and CO_2 (Figure 1(b)). For the generation of SVF spheroids, containing an identical cell number as the MVF spheroids, we seeded ~30,000 single cells into each well (Figure 1(b)). During spheroid generation, the culture medium was changed 2 days after seeding. After 5 days, the spheroids were harvested and their diameters were measured by analyzing light microscopic images using FIJI software (NIH, Bethesda, MD, USA).

Scanning electron microscopy (SEM)

The surface topography of MVF and SVF spheroids was visualized by SEM as previously described in detail.[22] Briefly, the spheroids were washed and subsequently fixed in 2% (v/v) glutardialdehyde in 0.1 M sodiumcacodylate buffer for 10 min at room temperature (RT). The spheroids were incubated in osmium tetroxide (1% (v/v) in 0.2 M sodiumcacodylate buffer) and dehydrated by incubation in an ethanol series. After washing, the dried samples were transferred to conductive carbon adhesive tabs and analyzed in a FEI XL 30 ESEM FEG SEM device (FEI, Hillsboro, OR).

Neutral red, trypan blue and propidium iodide (PI) staining

To analyze the number of dead cells, we stained SVF single cells and MVF from three mice directly after their isolation for 10 min with 2 µg/mL PI and 2 µg/mL Hoechst 33342 at RT. The stained cells were transferred to a slide, sealed with a coverslip and visualized by fluorescence microscopy using the 20× objective of a BX60 microscope (Olympus). We analyzed five high power fields (HPF) per slide and the number of PI-positive cells per HPF was given in % of all analyzed cells.

For neutral red and trypan blue stainings, spheroids were incubated for 2 min at RT and subsequently washed with phosphate-buffered saline (PBS). The cellular stainings were visualized in bright field using a BZ-8000 microscope (Keyence).

Flow cytometry

The viability of cells within MVF and SVF spheroids was determined by flow cytometry of PI- and Annexin V-stained cells as described previously.[23] For this purpose, the spheroids were dispersed into single cells by Accutase®. The cells were stained for 15 min with PI (10 µg/mL) and Annexin V (100 µg/mL) according to the manufacturer's protocol (Roche). Finally, the cells were analyzed by flow cytometry using a FACScan (BD Biosciences). The numbers of viable (unstained), apoptotic (Annexin V-positive), necrotic (PI-positive) as well as necroptotic (PI- and Annexin V-double positive) cells were given in %.

To assess the expression of stem cell surface marker proteins, the spheroids were dispersed into single cells by Accutase® and subsequently incubated with phycoerythrin (PE)-labeled primary antibodies for 1 h at RT. Afterwards, the cells were washed in PBS and the number of PE-positive cells was analyzed by flow cytometry using a FACScan (BD Biosciences).

Sprouting assay

The angiogenic activity of MVF and SVF spheroids was determined by means of a sprouting assay as previously

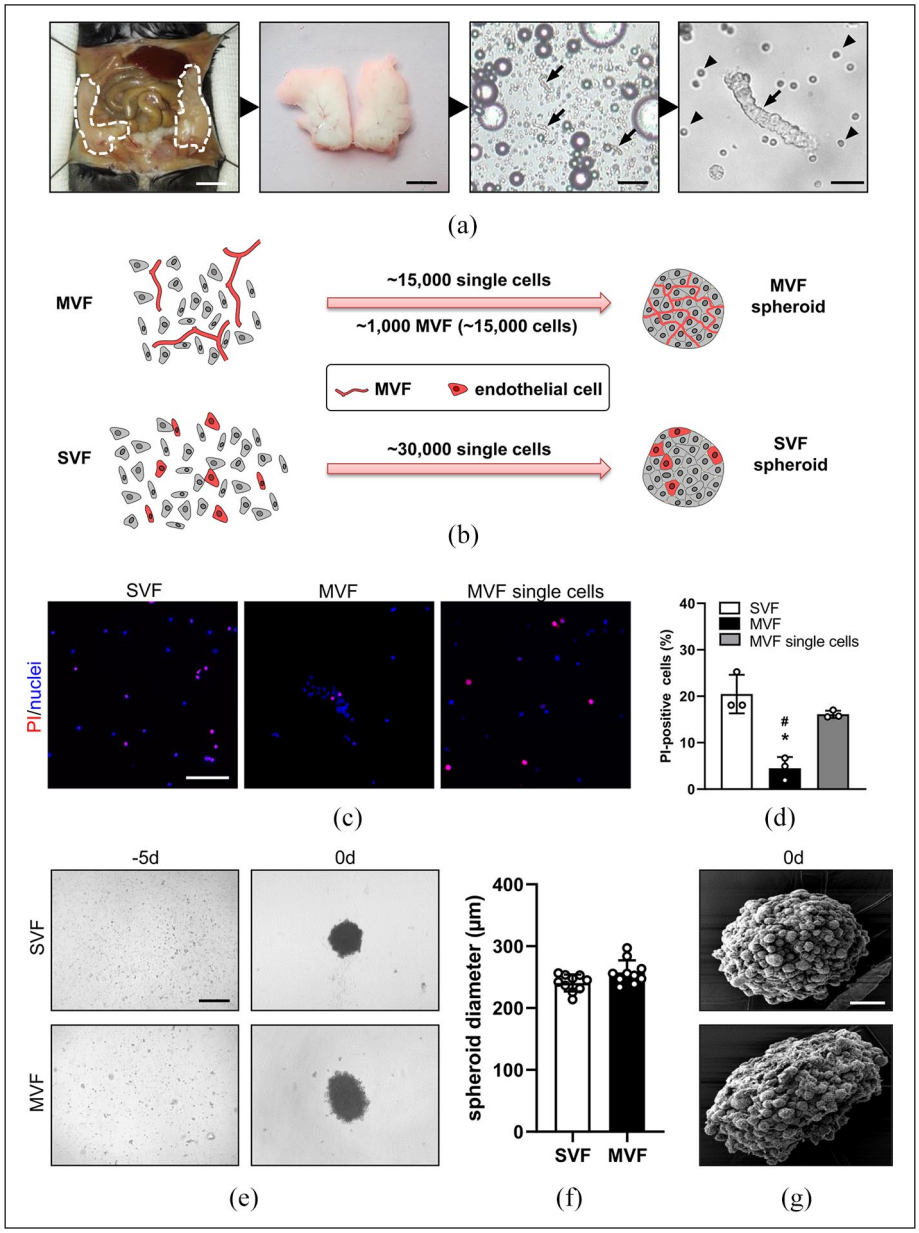

Figure 1. Generation of MVF and SVF spheroids: (a) generation of MVF isolates. The epididymal fat pads (left panel; borders marked by broken lines) of C57BL/6N donor mice were excised, washed, mechanically processed, and subsequently enzymatically digested. MVF are marked by arrows, single cells are marked by arrowheads. Scale bars (left to right panel): 5 mm, 10 mm, 120 µm, 25 µm, (b) schematic illustration of spheroid generation. For the generation of MVF spheroids, ~1000 MVF (each consisting of ~15 cells) and ~15,000 single cells were cultured by means of the liquid overlay technique for 5 days. For the generation of SVF spheroids, a comparable cell number of ~30,000 single cells were cultured by means of the liquid overlay technique for 5 days, (c) fluorescence microscopic images of propidium iodide-(red) and Hoechst 33342 (blue)-stained SVF single cells, MVF and the single cell fraction of MVF. Scale bar: 100 µm, (d) quantitative analysis of PI-positive cells (in % of all Hoechst 33342-positive cells per HPF) within SVF single cells, MVF and the single cell fraction of MVF directly after their isolation. Mean ± SD ($n = 4$). *$p < 0.05$ versus SVF; #$p < 0.05$ versus MVF single cells, (e) generation of SVF and MVF spheroids by means of the liquid overlay technique on day −5 and day 0. Scale bar: 200 µm, (f) quantification of SVF and MVF spheroid diameters (µm) on day 0. Mean ± SD ($n = 10$), and (g) morphology of SVF and MVF spheroids on day 0 represented by SEM images. Scale bar: 40 µm.

described in detail.[24] Briefly, the spheroids were collected on day 0 (directly after generation), resuspended in a collagen solution and transferred in a 24-well plate. DMEM was added to the wells and the spheroids were incubated for 3 days at 37°C and 5% CO_2. The cumulative length of the sprouts (µm) that grew out of each spheroid was measured on days 0, 1, and 2 by means of ImageJ software (NIH, Bethesda, MD, USA).

Oil Red O staining

MVF and SVF spheroids were seeded on cell culture dishes and cultured for 5 days in DMEM supplemented with 2 µM insulin at 37°C and 5% CO_2. To stain the lipid droplets of outgrowing pre-adipocytes and adipocytes, the spheroids were stained with Oil Red O as previously described.[25] Briefly, the spheroids were fixed, incubated for 5 min in 60% isopropanol and subsequently incubated for 1 h in filtered Oil Red O working solution. The stained lipid droplets were visualized with a BX60 microscope (Olympus).

Dorsal skinfold chamber model and spheroid transplantation

The in vivo vascularization of transplanted spheroids was analyzed by means of the dorsal skinfold chamber model as previously described in detail.[26] Briefly, two symmetrical titanium frames were implanted on the extended dorsal skinfold of 16 anesthetized C57BL/6N mice. One skin layer including skin, subcutis, and the retractor muscle was completely removed in a circular area with a diameter of ~15 mm. This area was covered by a removable cover slip and a snap ring to provide direct microscopic access to the microcirculation of the tissue. Afterwards, the animals were allowed to recover from the surgical procedure for 72 h. For the transplantation of spheroids, the cover slip was removed and the tissue was washed with saline. Thereafter, seven MVF or SVF spheroids were transplanted onto the striated muscle tissue within each chamber ($n = 8$ animals per group).

Intravital fluorescence microscopy

To visualize the microcirculation, mice with a dorsal skinfold chamber were anesthetized and retrobulbarily injected with 0.05 mL 5% FITC-dextran for contrast enhancement by staining of blood plasma. The mice were positioned under a fluorescence microscope (Zeiss) with a 100 W mercury lamp attached to a blue filter block (excitation wavelength: 450–490 nm/emission wavelength: >515 nm) to visualize the microcirculation within the chamber. The microscopic images were recorded by a charge-coupled device video camera (FK6990; Pieper) and transferred to a monitor with a DVD system for further off-line evaluation.

The microscopic images were analyzed by the computer-assisted image analysis system CapImage (Zeintl, Heidelberg, Germany) as described previously in detail.[27,28] Briefly, during the post-transplant time course, the functional microvessel density (cm/cm²) was determined as the total length of all red blood cell (RBC)-perfused microvessels per spheroid area and the vascularized area was given in % of the initial spheroid area (day 0). Moreover, we determined the take rate (%), which is the fraction of engrafted spheroids in relation to all transplanted spheroids per chamber on day 10. Finally, microhemodynamic parameters, including the diameter (µm), the centerline red blood cell (RBC) velocity (µm/s), and the volumetric blood flow (pL/s), of four to eight individual microvessels within the spheroids were analyzed.[27,28]

Immunohistochemistry

The cellular composition of MVF and SVF spheroids was assessed by immunohistochemistry. For this purpose, 20 spheroids (each) were embedded in a mixture of 100 µL HepatoQuick®, 50 µL human citrate plasma and 10 µL of 10% $CaCl_2$. The resulting clots were fixed for 24 h in 4% paraformaldehyde at 4°C. The samples were then dehydrated, embedded in paraffin, and cut into 3-µm-thick sections. The tissue slices were stained with specific primary antibodies (anti-CD31, anti-α-SMA, anti-casp-3, anti-Ki67), which were detected by their corresponding secondary antibodies and visualized by a BX60 fluorescence microscope (Olympus). The number of positive-stained cells (mean of three slices per spheroid) was given in % of all spheroid cells.

For the preparation of histological sections, specimens of spheroid-containing dorsal skinfold chamber preparations from five mice containing at least three transplanted spheroids were fixed for 24 h in 4% formalin. The formalin-fixed specimens were then embedded in paraffin and 3-µm-thick sections were cut. For immunohistochemical analyses, the sections were stained with anti-CD31 and anti-α-SMA antibodies, which were detected by corresponding fluorescence-coupled secondary antibodies. Cell nuclei were stained with Hoechst 33342. The sections were analyzed by means of fluorescence microscopy. Moreover, the sections were stained with a myeloperoxidase (MPO) antibody followed by a biotinylated secondary antibody. The sections were counterstained with Mayer's hemalum solution and examined by light microscopy. The numbers of CD31-positive, α-SMA-positive, and MPO-positive cells were counted on three sections per spheroid using ImageJ software (NIH, Bethesda, MD, USA) and are given in % of all cells per spheroid area.

Statistical analysis

After testing the data for normal distribution and equal variance, differences between MVF and SVF spheroids were assessed by the unpaired Student's *t*-test (Prism 8 software, GraphPad, USA). In case of non-parametric data, differences between the two groups were assessed by the Mann-Whitney rank sum test. All values are expressed as mean ± standard deviation (SD). Statistical significance was accepted for $p < 0.05$.

Results

Generation of MVF and SVF spheroids

For the isolation of MVF, the epididymal fat pads of C57BL/6N donor mice were mechanically and enzymatically processed. SVF single cells were obtained by an additional digestion step. To assess cell death induced by the isolation procedure, we analyzed the number of PI-positive cells in the SVF, MVF, and the single cell fraction of the MVF isolates (Figure 1(c)). Of interest, we found a significantly lower number of PI-positive cells in MVF when compared to SVF and the single cell fraction of the MVF isolates (Figure 1(d)).

For the generation of MVF spheroids, ~1000 MVF (each consisting of ~15 cells) and ~15,000 single cells were cultured by means of the liquid overlay technique for 5 days. SVF spheroids consisted of a comparable cell number of ~30,000 single cells. This resulted in compact and roundly shaped spheroids with a rough and heterogeneous surface pattern (Figure 1(e) and (f)). Of note, MVF and SVF spheroids exhibited a comparable diameter of ~250 µm (Figure 1(g)).

Viability of MVF and SVF spheroids

To analyze the viability of MVF and SVF spheroids, we performed neutral red and trypan blue stainings (Figure 2(a)). We found that MVF and SVF spheroids are positive for neutral red and negative for trypan blue without any differences between the two groups. In contrast, H_2O_2-treated MVF and SVF spheroids stained positive for trypan blue, negative for neutral red and were larger than non-treated spheroids. The latter observation is caused by H_2O_2-induced necrosis and apoptosis, which leads to various morphological cell death features, such as cell swelling and the loss of membrane integrity.

Moreover, we analyzed the viability of the spheroids by flow cytometry of PI- and Annexin V-positive cells (Figure 2(b) and (c)). As expected, we detected a comparably high number of vital cells and low numbers of necrotic, apoptotic, and necroptotic cells in MVF and SVF spheroids, which also did not differ between the two groups. Additional immunohistochemical analyses revealed that MVF and SVF spheroids contain a comparable fraction of ~7% Ki67-positive proliferating cells and <1% casp-3-positive apoptotic cells (Figure 2(d)–(g)).

To characterize the cellular composition of SVF and MVF spheroids, we additionally examined the expression of progenitor cell markers by flow cytometry. We found that the two spheroid types contain ~40% CD73-positive cells and ~20% CD117-positive cells (Figure 2(h)). In contrast, we detected a comparably low number (~2%) of CD29-positive cells (Figure 2(h)).

Angiogenic activity of MVF and SVF spheroids

We next analyzed the distribution of endothelial and perivascular cells within the spheroids by means of immunohistochemistry (Figure 3(a)). We detected CD31-positive capillary-like structures within the MVF spheroids, which were partly surrounded by α-SMA-positive perivascular cells. In contrast, SVF spheroids exhibited a random distribution of single CD31- and α-SMA-positive cells (Figure 3(a)). Quantitative analyses of these stainings revealed a significantly higher fraction of endothelial and perivascular cells in MVF spheroids when compared SVF spheroids (Figure 3(b) and (c)). To study the angiogenic activity of the two spheroid types, we performed a spheroid sprouting assay over 2 days (Figure 3(d)). In this assay, newly formed angiogenic sprouts, which consisted of CD31-positive endothelial cells surrounded by α-SMA-positive perivascular cells (Figure 3(d)), rapidly grew out of both MVF and SVF spheroids. Of note, this outgrowth was more pronounced in the MVF spheroids when compared to SVF controls (Figure 3(e)).

Beside endothelial and perivascular cells, MVF and SVF single cells contain various progenitor cells, including adipose tissue-derived stem cells (ADSC).[17,29] It has been shown that the combination of endothelial cells and ADSC is more effective in inducing neovascularization than either endothelial cells or ADSC alone.[30] Therefore, we further analyzed whether ADSC may contribute to the herein observed higher angiogenic potential of MVF. For this purpose, MVF and SVF spheroids were treated with insulin for 5 days to stimulate the formation of Oil Red O-positive lipid droplets within pre-adipocytes (Figure 3(f)). Of interest, we detected a substantial number of Oil Red O-positive cells within both groups. However, the fractions of these cells did not differ between the two groups over time (Figure 3(g)), indicating that ADSC do not contribute to the high angiogenic activity of MVF spheroids.

Vascularization of transplanted MVF and SVF spheroids

To evaluate the angiogenic activity of MVF and SVF spheroids in vivo, we implanted dorsal skinfold chambers in C57BL/6N recipient mice and transplanted seven neutral red-stained SVF or MVF spheroids onto the striated skin muscle tissue within the chamber observation window (Figure 4(a) and (b)). The engraftment of the spheroids was assessed by means of intravital fluorescence microscopy on days 0, 3, 6, and 10 (Figure 4(c) and (d)). In both groups we observed a progressively increasing functional microvessel density from day 0 to 6, which was not further elevated between day 6 and 10 (Figure 4(e)). The functional microvessel density of MVF spheroids was significantly higher on day 3 when compared to that of SVF

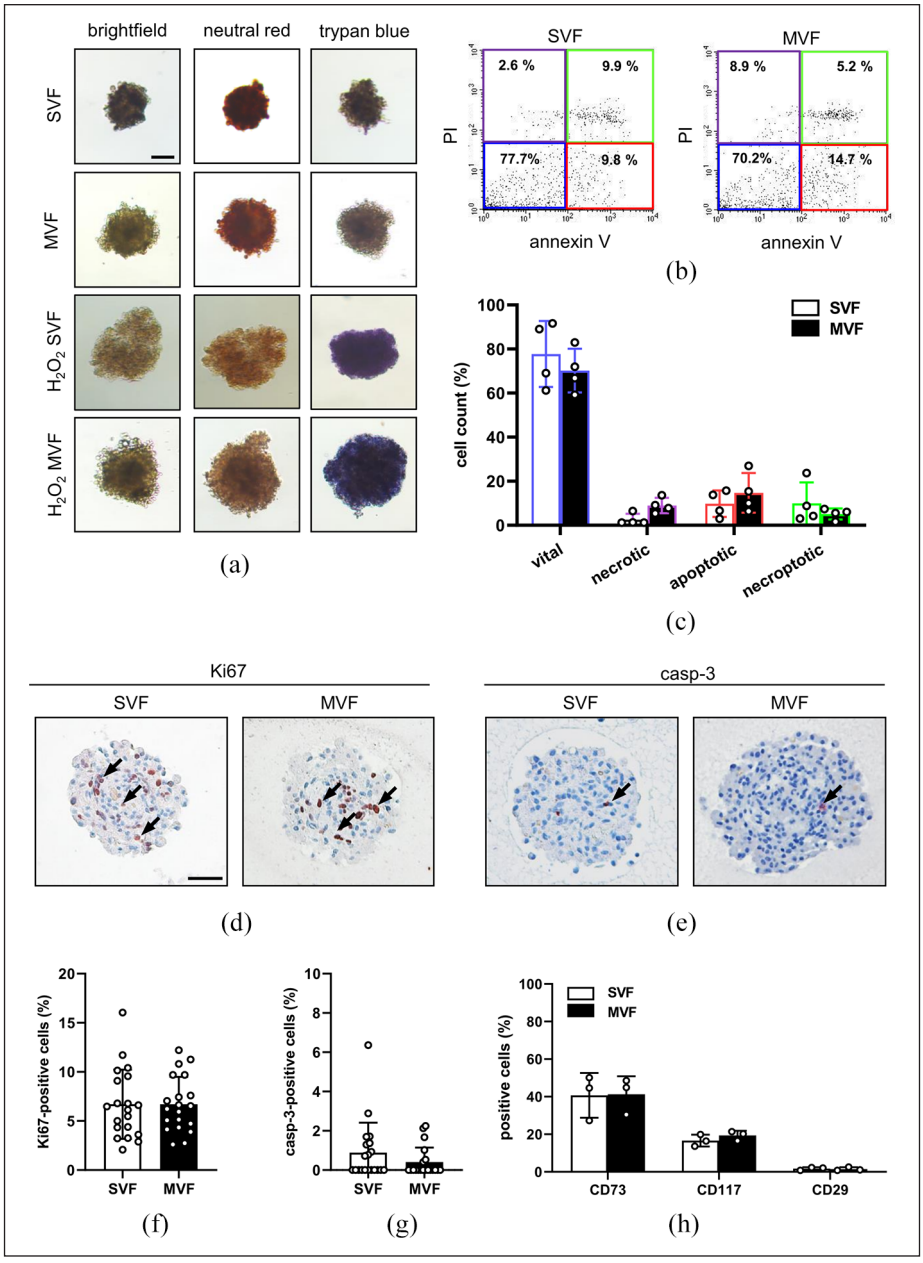

Figure 2. Viability of MVF and SVF spheroids: (a) representative neutral red and trypan blue stainings of SVF and MVF spheroids. MVF and SVF spheroids incubated for 10 h with 0.2% H_2O_2 served as positive controls. Scale bar: 150 µm, (b) representative flow cytometric scatterplots of PI/annexin V-stained cells from SVF and MVF spheroids, (c) quantitative analysis of PI/annexin V-stained cells (in % of total cell count) from SVF and MVF spheroids, as assessed by flow cytometry subdivided in vital, necrotic, apoptotic, and necroptotic cells. Mean ± SD ($n = 4$), (d, e) representative immunohistochemical stainings of Ki67-positive and casp-3-positive cells (marked by arrows) in SVF and MVF spheroids. Scale bar: 50 µm, (f, g) quantitative analysis of Ki67-positive and casp-3-positive cells (in % of all spheroid cells per HPF) in SVF and MVF spheroids. Mean ± SD ($n = 20$), and (h) quantitative analysis of CD73, CD117, and CD29 (in % of total cell count) within SVF and MVF spheroids, as assessed by flow cytometry. Mean ± SD ($n = 3$).

spheroids (Figure 4(e)). Moreover, we measured a larger vascularized area in the MVF group during the entire observation period (Figure 4(f)). The take rate of MVF spheroids was also significantly higher when compared to SVF spheroids (Figure 4(g)). In contrast, we did not detect any differences in the diameter, centerline RBC velocity, and volumetric blood flow of individual microvessels within the grafts (Figure 4(h)–(j)).

At the end of the in vivo experiments, we additionally analyzed the grafted spheroids by immunohistochemistry (Figure 5(a)). We detected a significantly higher number of CD31- and α-SMA-positive cells within the MVF spheroids compared to the SVF spheroids (Figure 5(a)–(c)). This is in line with our in vitro analyses showing more capillary-like structures within the MVF spheroids. Moreover, we determined the number of infiltrated MPO-positive neutrophils

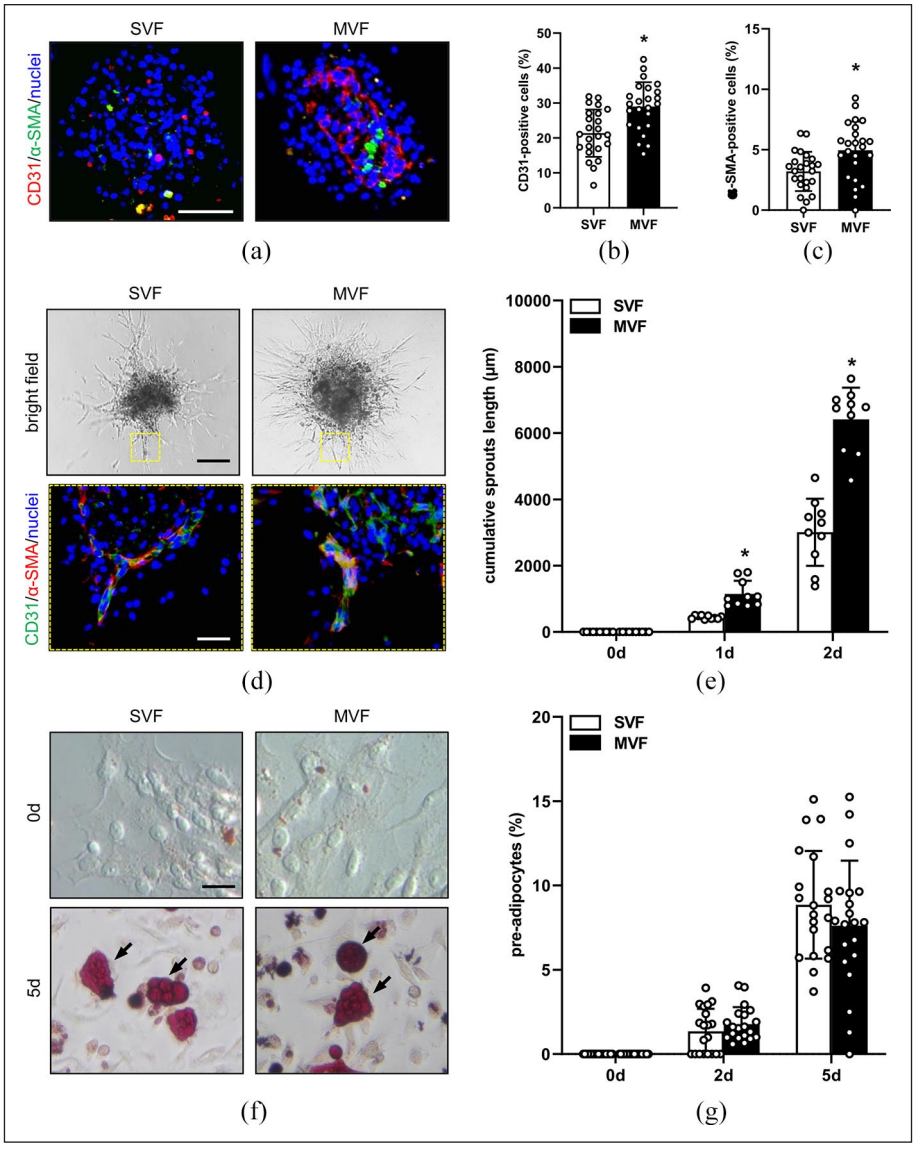

Figure 3. Angiogenic activity of MVF and SVF spheroids in vitro: (a) representative immunofluorescence stainings of CD31-positive endothelial cells (red) and α-SMA-positive perivascular cells (green) in SVF and MVF spheroids. Cell nuclei are stained with Hoechst 33342 (blue). Scale bar: 60 µm, (b, c) quantitative analysis of CD31- (b) and α-SMA-positive cells (c) (in % of all Hoechst 33342-positive spheroid cells per HPF) from SVF and MVF spheroids. Mean ± SD ($n = 25$). *$p < 0.05$ versus SVF, (d) bright field images of sprouting SVF and MVF spheroids on day 2. Scale bar: 150 µm. Yellow inserts: immunofluorescence stainings of CD31-positive endothelial cells (green) and α-SMA-positive perivascular cells (red) within the sprouts. Cell nuclei are stained with Hoechst 33342 (blue). Scale bar: 25 µm, (e) quantitative analysis of the cumulative sprouts length (µm) of SVF and MVF spheroids. Mean ± SD ($n = 10$). *$p < 0.05$ versus SVF, (f) bright field images of outgrowing cells from cultivated SVF and MVF spheroids on day 0 (unstained cells) and day 5 (arrows: Oil Red O-stained pre-adipocytes). Scale bar: 30 µm, and (g) quantitative analyses of Oil Red O-stained pre-adipocytes (in % of all cells per HPF) outgrowing from cultivated SVF and MVF spheroids on days 0, 2, and 5. Mean ± SD ($n = 20$).

within the grafts. However, we did not detect any differences between the two groups (Figure 5(d)).

Discussion

The present study demonstrates that it is feasible to generate stable spheroids out of MVF isolates, which consist of functional vessel segments and single cells. These spheroids exhibit a stronger angiogenic activity and an improved in vivo vascularization capacity when compared to SVF spheroids. Hence, they may serve as potent vascularization units in future tissue engineering applications.

During the last decades, several methods have been established for the fusion of single cells into spheroids,

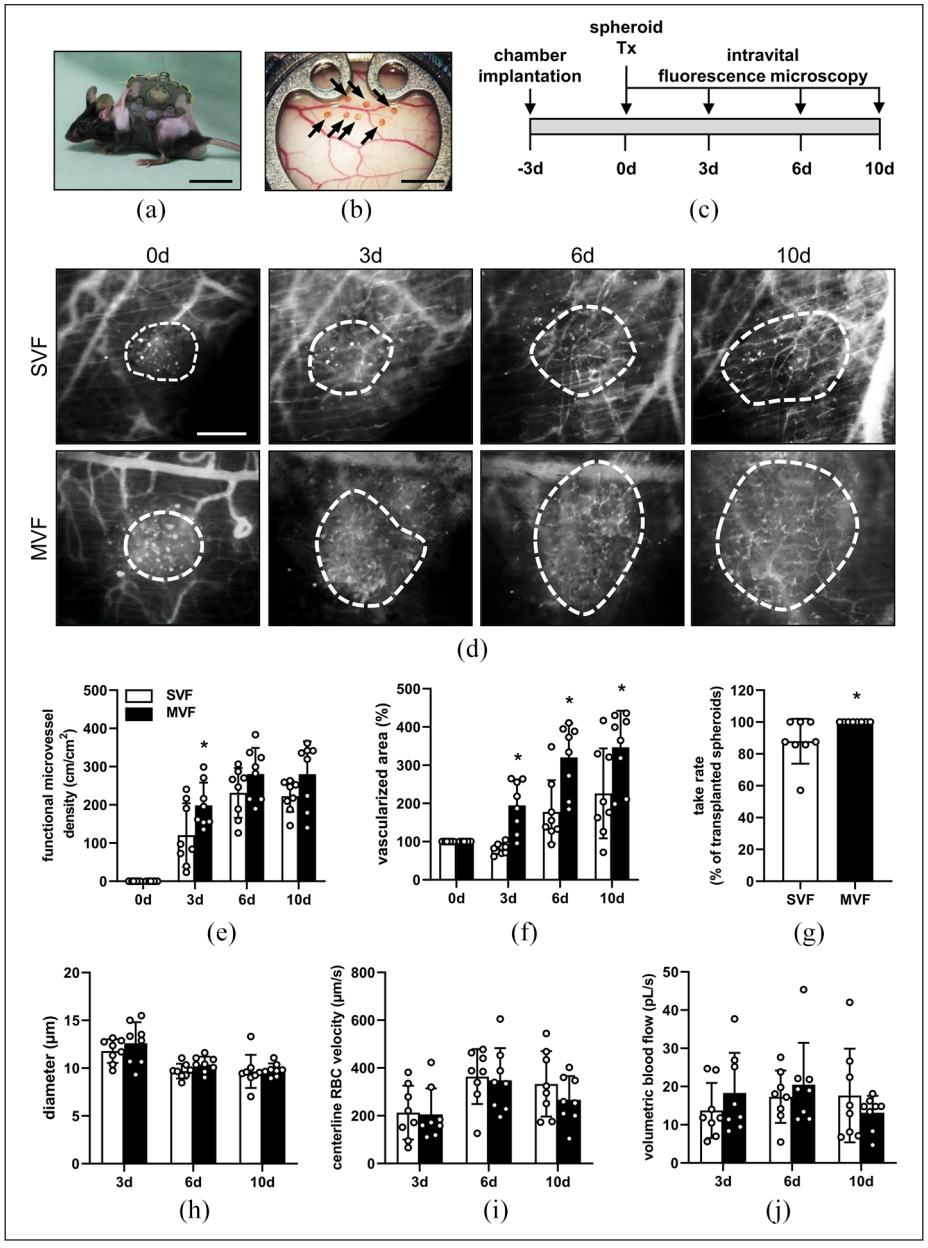

Figure 4. Angiogenic activity of MVF and SVF spheroids in vivo: (a) C57BL/6N mouse with an implanted dorsal skinfold chamber. Scale bar: 30 mm, (b) observation window of a dorsal skinfold chamber with seven transplanted, neutral red-stained MVF spheroids on day 0 (marked by arrows). Scale bar: 2.5 mm, (c) schematic illustration of the experimental in vivo setting. Dorsal skinfold chambers were implanted on day −3. MVF and SVF spheroids were transplanted onto the striated muscle tissue within the chamber on day 0. Intravital fluorescence microscopy was performed on days 0, 3, 6, and 10, (d) representative intravital fluorescence microscopic images of SVF and MVF spheroids within the dorsal skinfold chamber at the indicated time points. FITC-labeled dextran was intravenously injected to visualize blood vessel perfusion. The vascularized area of the spheroids is marked by broken white lines. Scale bar: 150 µm, (e, f) quantitative analysis of the functional microvessel density (cm/cm^2) (e) and vascularized area (in % of day 0) (f) of transplanted SVF and MVF spheroids on days 0, 3, 6, and 10 after transplantation into the dorsal skinfold chamber. Mean ± SD ($n = 8$). *$p < 0.05$ versus SVF, (g) take rate of spheroids (in % of all transplanted spheroids on day 0) on day 10. Mean ± SD ($n = 8$). *$p < 0.05$ versus SVF, and (h–j) quantitative analysis of the diameter (µm) (h), centerline RBC velocity (µm/s) (i), and volumetric blood flow (pL/s) (j) of newly formed microvessels within SVF and MVF spheroids after transplantation into the dorsal skinfold chamber on days 3, 6, and 10. Mean ± SD ($n = 8$).

such as the hanging drop or the liquid overlay technique.[31] The latter one is described as the most suitable approach for the generation of homogeneous spheroids consisting of different cell types.[31,32] Because SVF and MVF isolates are a heterogenous mixture of endothelial cells, pericytes, macrophages, fibroblasts, and ADSC,[19,29,33] we used the

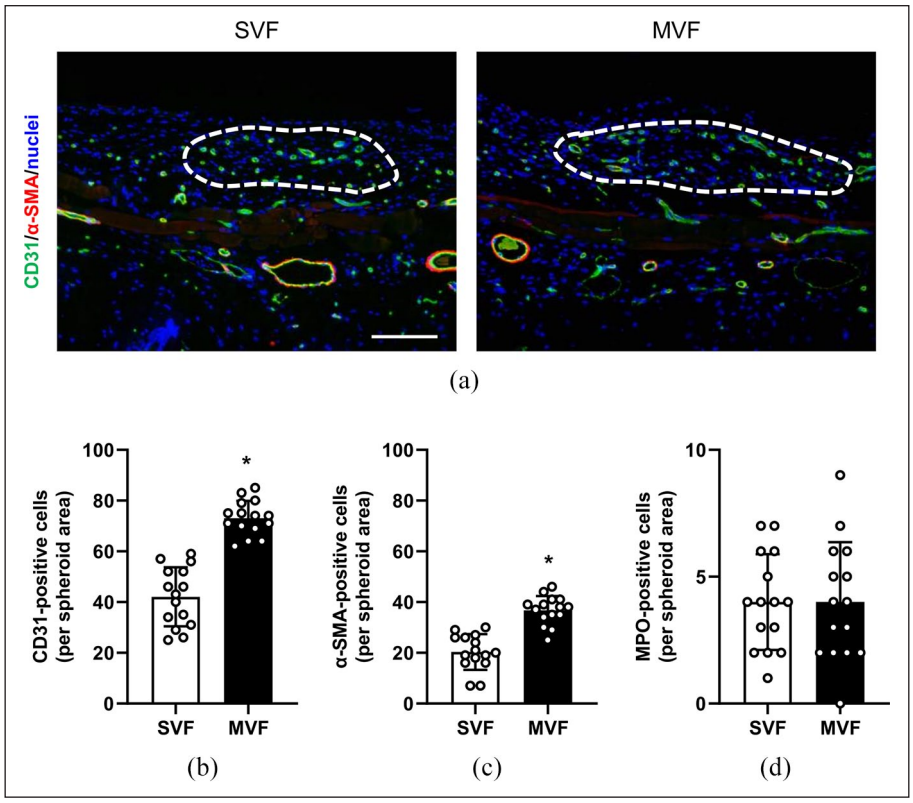

Figure 5. Immunohistochemical analyses of transplanted spheroids: (a) immunofluorescence stainings of CD31 (green) and α-SMA (red) within transplanted SVF and MVF spheroids (borders marked by broken white lines) on day 10 after transplantation into dorsal skinfold chambers. Cell nuclei are stained with Hoechst 33342 (blue). Scale bar: 50 µm, (b, c) quantitative analyses of CD31- (b) and α-SMA-positive cells (c) (in % of all Hoechst 33342-positive spheroid cells per spheroid area) within the SVF and MVF spheroids of immunohistochemical sections. Mean ± SD ($n = 15$). *$p < 0.05$ versus SVF, and (d) quantitative analysis of MPO-positive cells (in % of all spheroid cells per spheroid area) within the SVF and MVF spheroids of immunohistochemical sections. Mean ± SD ($n = 15$).

liquid overlay technique in the present study. By this, we generated compact, roundly, and viable SVF and MVF spheroids of comparable size within 5 days. Notably, the two spheroid types did neither differ in their cell viability nor in the number of Ki67-positive proliferative cells and casp-3-positive apoptotic cells.

Of interest, immunohistochemical stainings revealed a dense network of CD31-positive capillary-like structures within MVF spheroids, while SVF spheroids only contained randomly distributed single endothelial cells. Additional quantitative analyses showed a significantly higher number of endothelial cells and α-SMA-positive perivascular cells in MVF spheroids. In line with this finding, we also detected significantly less PI-positive necrotic cells in MVF when compared to SVF single cells and the fraction of MVF-associated single cells. The latter result may be explained by the fact that the close cell-cell contacts within intact tissue fragments, such as MVF, preserve cell viability.[34] Hence, it may be assumed that during the 5-day period of spheroid generation, more endothelial and perivascular cells survive within MVF spheroids when compared to SVF spheroids.

To test the angiogenic activity of MVF and SVF spheroids in vitro, we performed collagen-based sprouting assays. Of interest, angiogenic sprouting out of MVF spheroids was more pronounced when compared to SVF spheroids. This result may be explained by the higher number of endothelial cells and microvascular structures in MVF spheroids. The extracellular matrix (ECM) has also been shown to have a strong impact on angiogenesis.[35] Therefore, retained ECM components of individual MVF may have further contributed to the high angiogenic activity of MVF spheroids. On the other hand, MVF and SVF isolates also contain ADSC, a population of multipotent progenitor cells, which can be identified by insulin-stimulated differentiation into pre-adipocytes.[36] ADSC are known to promote angiogenesis and protect co-transplanted cells from inflammatory cytokine-induced cell death.[37,38] Therefore, we additionally assessed the fraction of pre-adipocytes in MVF and SVF spheroids. We did not detect a difference between the two spheroid types, which is in line with our flow cytometric analyses showing an equal expression of the progenitor cell markers CD117, CD73, and CD29 in the two spheroid types. These results

indicate that ADSC are not responsible for the improved angiogenic activity of MVF spheroids when compared to SVF spheroids.

To further assess the vascularization of MVF and SVF spheroids in vivo, we used the mouse dorsal skinfold chamber model, which is suitable to study the formation of new blood vessels in transplanted tissues by means of repetitive intravital fluorescence microscopy.[39] We measured a significantly higher functional microvessel density in MVF spheroids on day 3 when compared to SVF spheroids. Moreover, the vascularized area was markedly elevated in the MVF group during the entire in vivo observation period. Additional immunohistochemical stainings revealed a higher number of mature microvessels within MVF spheroids on day 10 when compared to SVF spheroids. These findings can be explained by the fact that MVF spheroids contain fully functional vessel segments, which rapidly interconnect with each other and the surrounding host microvasculature after transplantation. In contrast, SVF spheroids solely consist of single cells, which first need to reassemble into vessel-like structures to enable blood perfusion of the grafts.[40] Accordingly, SVF spheroids exhibited a delayed vascularization, which may also explain their reduced take rate when compared to MVF spheroids. In addition, we detected a slightly decreased vascularized area in the SVF group on day 3 when compared to day 0, which may be caused by the reduced angiogenic activity of the SVF spheroids during the initial posttransplant phase and, thus, hypoxia-induced cell death.

The herein described MVF spheroids may be used for different clinical applications in the future. For instance, they may ideally serve as vascularization units for implanted biomaterials and tissue constructs or for the improvement of wound healing. Moreover, they may also be suitable to study the pro- and anti-angiogenic effects of novel drugs by means of the spheroids-on-a-chip technology.[41] In this study, we used the liquid overlay technique for the fabrication of spheroids, which allows a precise control of the spheroid size by using defined numbers of SVF and MVF. However, this technique is time-consuming and, thus, difficult to implement into clinical practice. Accordingly, novel high-yield fabrication strategies for the generation of spheroids have to be established. In this context, Wassmer et al.[31] introduced the Sphericalplate 5D™, which consists of 12 wells with 750 micro cavities per well. This enables the generation of up to 9000 organoids per plate.

Conclusion

In this proof-of-principle study, we report for the first time the generation of stable spheroids out of MVF isolates. These spheroids exhibit a high vascularization potential due to their intrinsically preformed microvasculature. Of interest, we have recently shown that factors such as insulin-like growth factor (IGF-1) or erythropoietin (EPO) improve the vascularization capacity of MVF.[42,43] Hence, the exposure of MVF spheroids to IGF-1 or EPO prior to their transplantation may further boost their excellent vascularization properties. In addition, it should be considered that MVF spheroids also contain a substantial number of ADSC, which can be differentiated into various cell lineages, including adipocytes, osteoblasts, chondrocytes, and myocytes.[44] Accordingly, MVF spheroids may offer the exciting opportunity to generate prevascularized tissue-specific building blocks for tissue engineering.

Acknowledgements

We are grateful for the excellent assistance of Caroline Bickemann and Ruth M. Nickels. We acknowledge support by the Deutsche Forschungsgemeinschaft (DFG, German Research Foundation) and Saarland University within the funding programme Open Access Publishing.

Author contributions

LN, DM, SW, WM, and EA performed the experiments. MDM and WM provided essential material. LN, DM, SW, EA, and MWL designed experiments and analyzed and interpreted the data. LN and EA prepared the figures and EA, LN, MDM, and MWL wrote the manuscript. All authors have read and approved the submitted manuscript.

Availability of data and materials

All data can be obtained in this manuscript.

Declaration of conflicting interests

The author(s) declared no potential conflicts of interest with respect to the research, authorship, and/or publication of this article.

Ethical approval

This study was approved by the local governmental animal protection committee (Landesamt für Verbraucherschutz, Saarbrücken; permission number: 18/2017) and conducted in accordance with the Directive 2010/63/EU and the NIH Guidelines for the Care and Use of Laboratory Animals (NIH Publication #85-23 Rev. 1985).

Funding

The author(s) received no financial support for the research, authorship, and/or publication of this article.

ORCID iDs

Matthias W Laschke https://orcid.org/0000-0002-7847-8456
Emmanuel Ampofo https://orcid.org/0000-0002-1886-5657

References

1. Robert AW, Azevedo Gomes F, Rode MP, et al. The skin regeneration potential of a pro-angiogenic secretome from human skin-derived multipotent stromal cells. *J Tissue Eng* 2019; 10: 2041731419833391.

2. Peticone C, Thompson DS, Dimov N, et al. Characterisation of osteogenic and vascular responses of hMSCs to Ti-Co doped phosphate glass microspheres using a microfluidic perfusion platform. *J Tissue Eng* 2020; 11: 204173 1420954712.
3. Laschke MW and Menger MD. Life is 3D: boosting spheroid function for tissue engineering. *Trends Biotechnol* 2017; 35: 133–144.
4. Ryu NE, Lee SH and Park H. Spheroid culture system methods and applications for mesenchymal stem cells. *Cells* 2019; 8: 1620.
5. Laschke MW and Menger MD. Spheroids as vascularization units: from angiogenesis research to tissue engineering applications. *Biotechnol Adv* 2017; 35: 782–791.
6. Alajati A, Laib AM, Weber H, et al. Spheroid-based engineering of a human vasculature in mice. *Nat Methods* 2008; 5: 439–445.
7. Heo DN, Hospodiuk M and Ozbolat IT. Synergistic interplay between human MSCs and HUVECs in 3D spheroids laden in collagen/fibrin hydrogels for bone tissue engineering. *Acta Biomater* 2019; 95: 348–356.
8. Pitaktong I, Lui C, Lowenthal J, et al. Early vascular cells improve microvascularization within 3D cardiac spheroids. *Tissue Eng Part C Methods* 2020; 26: 80–90.
9. Chang WG, Andrejecsk JW, Kluger MS, et al. Pericytes modulate endothelial sprouting. *Cardiovasc Res* 2013; 100: 492–500.
10. Laschke MW and Menger MD. Prevascularization in tissue engineering: current concepts and future directions. *Biotechnol Adv* 2016; 34: 112–121.
11. Cerino G, Gaudiello E, Muraro MG, et al. Engineering of an angiogenic niche by perfusion culture of adipose-derived stromal vascular fraction cells. *Sci Rep* 2017; 7: 14252.
12. Hu C, Zaitseva TS, Alcazar C, et al. Delivery of human stromal vascular fraction cells on nanofibrillar scaffolds for treatment of peripheral arterial disease. *Front Bioeng Biotechnol* 2020; 8: 689.
13. Brett E, Zielins ER, Chin M, et al. Isolation of CD248-expressing stromal vascular fraction for targeted improvement of wound healing. *Wound Repair Regen* 2017; 25: 414–422.
14. Mazo M, Cemborain A, Gavira JJ, et al. Adipose stromal vascular fraction improves cardiac function in chronic myocardial infarction through differentiation and paracrine activity. *Cell Transplant* 2012; 21: 1023–1037.
15. Muller S, Ader I, Creff J, et al. Human adipose stromal-vascular fraction self-organizes to form vascularized adipose tissue in 3D cultures. *Sci Rep* 2019; 9: 7250.
16. Frueh FS, Später T, Scheuer C, et al. Isolation of murine adipose tissue-derived microvascular fragments as vascularization units for tissue engineering. *J Vis Exp* 2017; 122: 55721.
17. McDaniel JS, Pilia M, Ward CL, et al. Characterization and multilineage potential of cells derived from isolated microvascular fragments. *J Surg Res* 2014; 192: 214–222.
18. Hoying JB, Boswell CA and Williams SK. Angiogenic potential of microvessel fragments established in three-dimensional collagen gels. *In Vitro Cell Dev Biol Anim* 1996; 32: 409–419.
19. Später T, Frueh FS, Nickels RM, et al. Prevascularization of collagen-glycosaminoglycan scaffolds: stromal vascular fraction versus adipose tissue-derived microvascular fragments. *J Biol Eng* 2018; 12: 24.
20. Laschke MW and Menger MD. Adipose tissue-derived microvascular fragments: natural vascularization units for regenerative medicine. *Trends Biotechnol* 2015; 33: 442–448.
21. Walser R, Metzger W, Gorg A, et al. Generation of co-culture spheroids as vascularisation units for bone tissue engineering. *Eur Cell Mater* 2013; 26: 222–233.
22. Laschke MW, Augustin VA, Sahin F, et al. Surface modification by plasma etching impairs early vascularization and tissue incorporation of porous polyethylene (Medpor®) implants. *J Biomed Mater Res B Appl Biomater* 2016; 104: 1738–1748.
23. Nalbach L, Roma LP, Schmitt BM, et al. Improvement of islet transplantation by the fusion of islet cells with functional blood vessels. *EMBO Mol Med* 2021; 13: e12616.
24. Heiss M, Hellstrom M, Kalen M, et al. Endothelial cell spheroids as a versatile tool to study angiogenesis in vitro. *FASEB J* 2015; 29: 3076–3084.
25. Schwind L, Nalbach L, Zimmer AD, et al. Quinalizarin inhibits adipogenesis through down-regulation of transcription factors and microRNA modulation. *Biochim Biophys Acta Gen Subj* 2017; 1861: 3272–3281.
26. Laschke MW, Vollmar B and Menger MD. The dorsal skinfold chamber: window into the dynamic interaction of biomaterials with their surrounding host tissue. *Eur Cell Mater* 2011; 22: 147–164; discussion 164–167.
27. Menger MD, Vajkoczy P, Leiderer R, et al. Influence of experimental hyperglycemia on microvascular blood perfusion of pancreatic islet isografts. *J Clin Invest* 1992; 90: 1361–1369.
28. Ampofo E, Rudzitis-Auth J, Dahmke IN, et al. Inhibition of protein kinase CK2 suppresses tumor necrosis factor (TNF)-α-induced leukocyte-endothelial cell interaction. *Biochim Biophys Acta* 2015; 1852: 2123–2136.
29. Lin CS, Xin ZC, Deng CH, et al. Defining adipose tissue-derived stem cells in tissue and in culture. *Histol Histopathol* 2010; 25: 807–815.
30. Traktuev DO, Prater DN, Merfeld-Clauss S, et al. Robust functional vascular network formation in vivo by cooperation of adipose progenitor and endothelial cells. *Circ Res* 2009; 104: 1410–1420.
31. Wassmer CH, Bellofatto K, Perez L, et al. Engineering of primary pancreatic islet cell spheroids for three-dimensional culture or transplantation: a methodological comparative study. *Cell Transplant* 2020; 29: 963689720937292.
32. Metzger W, Sossong D, Bachle A, et al. The liquid overlay technique is the key to formation of co-culture spheroids consisting of primary osteoblasts, fibroblasts and endothelial cells. *Cytotherapy* 2011; 13: 1000–1012.
33. Kilinc MO, Santidrian A, Minev I, et al. The ratio of ADSCs to HSC-progenitors in adipose tissue derived SVF may provide the key to predict the outcome of stem-cell therapy. *Clin Transl Med* 2018; 7: 5.
34. Wei Q, Hariharan V and Huang H. Cell-cell contact preserves cell viability via plakoglobin. *PLoS One* 2011; 6: e27064.

35. Mongiat M, Andreuzzi E, Tarticchio G, et al. Extracellular matrix, a hard player in angiogenesis. *Int J Mol Sci* 2016; 17: 1822.
36. Kim YW, Min HJ, Choi RJ, et al. Insulin promotes adipose-derived stem cell differentiation after fat grafting. *Plast Reconstr Surg* 2018; 142: 927–938.
37. Song L, Sun Z, Kim DS, et al. Adipose stem cells from chronic pancreatitis patients improve mouse and human islet survival and function. *Stem Cell Res Ther* 2017; 8: 192.
38. Cao Y, Sun Z, Liao L, et al. Human adipose tissue-derived stem cells differentiate into endothelial cells in vitro and improve postnatal neovascularization in vivo. *Biochem Biophys Res Commun* 2005; 332: 370–379.
39. Nalbach L, Schmitt BM, Becker V, et al. Nerve/glial antigen 2 is crucially involved in the revascularization of freely transplanted pancreatic islets. *Cell Tissue Res* 2019; 378: 195–205.
40. Koh YJ, Koh BI, Kim H, et al. Stromal vascular fraction from adipose tissue forms profound vascular network through the dynamic reassembly of blood endothelial cells. *Arterioscler Thromb Vasc Biol* 2011; 31: 1141–1150.
41. Khot MI, Levenstein MA, De Boer GN, et al. Characterising a PDMS based 3D cell culturing microfluidic platform for screening chemotherapeutic drug cytotoxic activity. *Sci Rep* 2020; 10: 15915.
42. Karschnia P, Scheuer C, Hess A, et al. Erythropoietin promotes network formation of transplanted adipose tissue-derived microvascular fragments. *Eur Cell Mater* 2018; 35: 268–280.
43. Laschke MW, Kontaxi E, Scheuer C, et al. Insulin-like growth factor 1 stimulates the angiogenic activity of adipose tissue-derived microvascular fragments. *J Tissue Eng* 2019; 10: 2041731419879837.
44. Rafols ME. Adipose tissue: cell heterogeneity and functional diversity. *Endocrinol Nutr* 2014; 61: 100–112.